International Journal of Non-Linear Mechanics 45 (2010) 837–849

Contents lists available at ScienceDirect

International Journal of Non-Linear Mechanics

journal homepage: www.elsevier.com/locate/nlm

Vibration reduction of the impact system by an SMA restraint: numerical studies

Elena Sitnikova [a], Ekaterina Pavlovskaia [a,*], Marian Wiercigroch [a], Marcelo A. Savi [b]

[a] Centre for Applied Dynamics Research, School of Engineering, University of Aberdeen, AB24 3UE Aberdeen, UK
[b] Department of Mechanical Engineering, Universidade Federal do Rio de Janeiro, COPPE, P.O. Box 68.503, 21.941.972 Rio de Janeiro, RJ, Brazil

ARTICLE INFO

Article history:
Received 15 October 2008
Received in revised form
21 September 2009
Accepted 30 November 2009

Keywords:
Non-smooth system
Non-linear dynamics
Chaos
Vibration reduction
Shape memory alloy
Smart materials

ABSTRACT

The dynamic behaviour of an impact oscillator with a shape memory alloy (SMA) restraint is modelled and analyzed. This impact oscillator has the secondary support made from an SMA and the thermo-mechanical description of the SMA element follows the formulation proposed by Bernardini et al. [1,2]. The thermo-mechanical coupling terms included in the energy balance equation allow to undertake the non-isothermal analysis. Due to the mechanical characteristics of the SMA element and the non-smooth nature of the impacts, five different modes of operation can be distinguished. The undertaken numerical investigations suggest that the system can exhibit complex dynamic responses, which if appropriately controlled can be used for vibration reduction. A comparison with an equivalent elastic oscillator is made. It is found out that the low amplitude regimes are not affected by the SMA element. On contrary, for the large amplitude responses, a significant vibration reduction may be achieved due to the phase transformation hysteresis loop. Various bifurcation scenarios are constructed and the influence of the SMA element is discussed. In particular, the analysis of the frequency and amplitude variations of the external excitation is given and the parameter ranges where the vibration reduction is possible are identified.

1. Introduction

Shape memory alloys (SMAs) are a class of metallic alloys which possesses attractive mechanical properties when subjected to stress and/or temperature changes. Basically, an SMA has two different solid phases: austenite, which is stable in stress-free state at high temperatures, and martenstite, which is a low-temperature stress-free state phase. The pseudoelastic behaviour in SMAs is observed above the critical temperature when in the equilibrium stress-free configuration austenite is stable. The schematic representation of the SMA pseudoelastic behaviour for the case of the uniaxial loading is depicted in Fig. 1a. Due to the applied load, the forward transformation from austenite to the martensite takes place; this corresponds to the upper plateau of the stress–strain curve. Similarly, when the unloading reverse transformation occurs, the material returns to the initial austenite state by a different path (the lower plateau of the stress–strain curve), forming a hysteresis. The values of the threshold forces of the phase transformations depend on the temperature; these temperature dependencies are depicted in Fig. 1b. This means that if a material is loaded at a temperature $\theta > A_f$, the transformation forces increase linearly with temperature as $f_{\theta_\alpha}(\theta) = b(\theta - \theta_\alpha)$, where $\theta_\alpha = M_f, M_s, A_s$ or A_f.

The other type of hysteretic behaviour is shown in Fig. 1c. It occurs as a result of temperature variation, when with heating martensite (or cooling austenite) the phase transformations begin once the temperature reaches the critical value $A_s(M_s)$ and ends at the temperature $A_f(M_f)$. These temperatures are the material constants and can be determined from standard tests.

Shape memory alloys are being used in various applications. It is fair to say that dynamical applications of SMAs are associated with both the adaptive dissipation of energy related to their hysteretic behaviour and large changes in their mechanical properties caused by phase transformations. These aspects can be explored both in the adaptive passive and the active control [3]. The dynamical responses of SMA systems have been previously studied treating the main aspects of smart systems with SMA devices. Adaptive–passive vibration control has been applied on bridges [4] and other civil structures subjected to earthquakes [5]. Systems with SMA elements or structures can exhibit complex dynamical responses including chaos and hyperchaos [2,6–8].

Martensitic transformation can be considered as a non-diffusive process for many practical situations where the heat transfer process is longer than the martensitic transformation, as it occurs at rates close to the speed of the material shear wave [9]. On the other hand, the phase transformation critical stresses are

* Corresponding author.
E-mail address: e.pavlovskaia@abdn.ac.uk (E. Pavlovskaia).

0020-7462/$ - see front matter © 2010 Elsevier Ltd. All rights reserved.
doi:10.1016/j.ijnonlinmec.2009.11.013

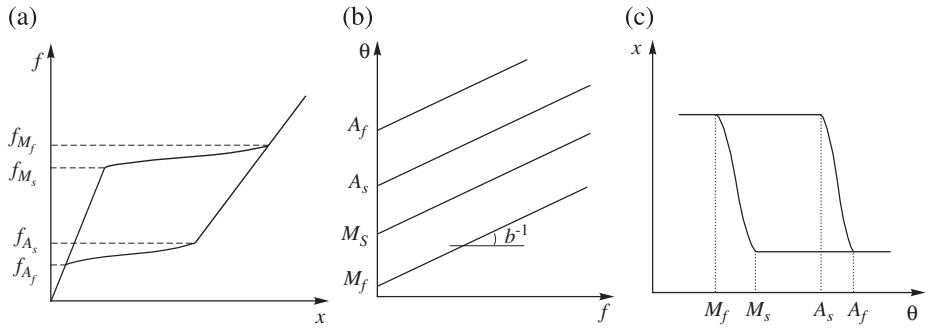

Fig. 1. Schematic representations of the basic properties of the SMA: (a) mechanical hysteresis (effect of pseudoelasticity), (b) temperature–stress diagram and (c) thermal hysteresis (temperature induced phase transformations).

temperature dependent and, as a consequence, the thermomechanical behaviour of SMA is affected by the loading rate. In this regard, the SMA behaviour is associated with the balance between the loading rate aspect and the thermomechanical coupling effect related to the latent heat of the phase transformation. Therefore, SMA devices have a rate-dependence characteristic that means that the thermomechanical response depends on loading rate [10,11]. This situation may be even more important to the SMA devices subjected to dynamical loadings. Bernardini and Rega [2] analyze different aspects concerning SMA dynamical systems and, among them, the influence of the environmental heat exchange in the dynamical response. Lagoudas et al. [12] presents experimental studies where temperature variations due to phase transformations are clearly identified. At the same time, the analysis of the SMA dynamical systems under isothermal conditions is also important as it allows to distinguish system behaviour caused by temperature variation [2], or even to prevent underestimation of damping properties [13].

An interesting SMAs application in dynamical systems is the an impact oscillator with SMA elements. A prototype of this kind of system capturing the most important features is an impact oscillator with the secondary support made from SMA. It is expected that the high dissipation capacity of SMA due to hysteresis loop will result in less complex behaviour, dramatically changing the system response when compared to those obtained with a linear elastic secondary support [14]. In terms of engineering applications, the use of SMA can potentially avoid dangerous transients. Besides, using an SMA support may avoid certain bifurcations, simplifying dynamical responses and allowing for an effective energy use. On the other hand, the study of the co-existence of attractors [15] reveals more complex behaviour for the impact oscillator with the pseudoelastic secondary constraint at the certain frequency ranges. It was shown that the presence of the SMA in the discontinuous support can eliminate some of the undesirable responses as well as it can generate the new high amplitude responses.

This paper deals with the non-linear dynamics of an impact oscillator having the secondary support made from an SMA. The thermomechanical behaviour of SMA is described by the constitutive model due to Bernardini and Rega [2]. Thermomechanical coupling terms are considered in the energy equation allowing the analysis of temperature evolution. A comparison with an equivalent impact oscillator having an elastic support is made establishing the influence of constitutive non-linearity on the system dynamics. The influence of the external excitation is studied by investigating situations where vibration reduction is achieved due to the phase transformation hysteresis. Various bifurcation scenarios are discussed to explore complex responses of both systems. Results show some cases where SMA support is useful for vibration reduction and others where this reduction is not possible.

The paper is organized as follows. The description of the physical model is presented in the Section 2 together with the equations of motion and the modes of motion in which the considered system may operate. Numerical results demonstrating some typical examples of the system behaviour are presented in the Section 3. Here the ranges of parameters where the vibration reduction can be achieved are discussed and dangerous scenarios of appearance of large amplitude pseudoelastic responses are shown. Finally, some conclusions are given.

2. Physical model, equations of motion and modes of motion

The dynamical system under consideration is the one degree-of-freedom piecewise smooth oscillator shown in Fig. 2a. The system consists of a mass m supported by a primary spring of stiffness K_1 and a damper μ. The oscillating mass collides with a motion restraint made of SMA having pseudoelastic behaviour. The gap between the mass and the SMA constraint in the equilibrium position is g. The external force in the form of harmonic excitation $F = A\cos(\Omega t)$ is applied to the base of the oscillator.

The considered system has two types of non-linearities. The first one is associated with the discontinuous characteristics caused by intermittent contacts, whereas of the second type of non-linearity is related to the pseudoelastic nature of SMA element. In order to examine the influence of the SMA on the dynamic response of such system, a comparison with equivalent oscillator shown in Fig. 2b with a plain elastic secondary support has been made. Such comparison is important because an impact oscillator alone has a very rich dynamical behaviour, and it will be shown that the use of the SMA can modify it quite drastically. For the sake of simplicity, the oscillators with SMA and elastic secondary support will be referred to in the future as "pseudoelastic" and "elastic" oscillators.

The equations of motion for the pseudoelastic and elastic oscillator are as follows:

$$m\ddot{x} + \mu\dot{x} + K_1 x + f_{pe}\mathrm{H}(-x-g) = A\Omega^2\cos(\Omega t), \tag{1}$$

$$m\ddot{x} + \mu\dot{x} + K_1 x + K(x+g)\mathrm{H}(-x-g) = A\Omega^2\cos(\Omega t), \tag{2}$$

where f_{pe} is a restoring force in the pseudoelastic element, and $\mathrm{H}(\cdot)$ is a Heaviside step function which is used to describe a piecewise smooth nature of the system. It takes the value of 1 during the contact of mass with the constraint, and the value of 0 otherwise.

The modelling of the behaviour of such system is completed by introducing the explicit expression for the pseudoelastic element restoring force f_{pe}. Consequently, the variations of temperature

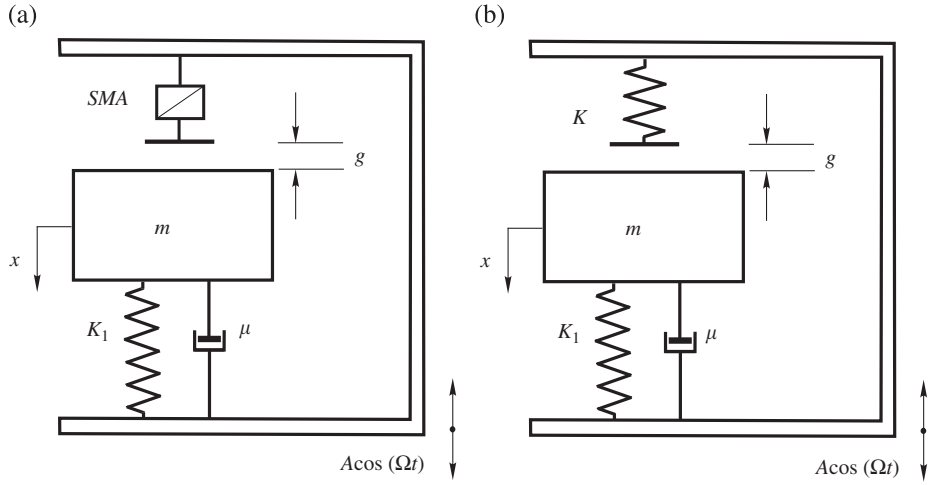

Fig. 2. Physical models of impact oscillators: (a) oscillator with SMA secondary support; (b) oscillator with elastic secondary support.

during phase transformation process in the SMA element have to be taken into account, and in this study the thermomechanical model developed for pseudoelastic SMA by Bernardini and Rega [2] is used.

The model proposed in [2] considers both the mechanical and thermal responses of the SMA element, which implies that along with the displacement x and velocity v, the temperature θ is considered as a state variable. The description of the phase transformation evolution is done by introducing the volume fraction of martensite ξ as an internal variable, with $\xi \in [0, 1]$. Zero value of ξ corresponds to SMA material being fully in the austenite phase and the one value corresponds to material being fully in martensite state. Then the set of equations of motion for the discontinuous pseudoelastic oscillator can be written as follows [15]:

$$\begin{aligned}
&\dot{x} = v,\\
&\dot{v} = -\frac{K_1}{m}x - \frac{\mu}{m}v - \frac{K}{m}(x+g-\delta\xi\,\mathrm{sign}(x+g))\mathrm{H}(-x-g) + \frac{A\Omega^2}{m}\cos(\Omega t),\\
&\dot{\xi} = \mathcal{H}(\xi,\xi_0)\left[Kv\ \mathrm{sign}(x+g) - \frac{bh(\theta_e-\theta)}{c}\right]\mathrm{H}(-x-g),\\
&\dot{\theta} = \left[\frac{\Lambda(\xi,\xi_0)+b\delta\theta}{c}\right]\dot{\xi}\mathrm{H}(-x-g) + \frac{h(\theta_e-\theta)}{c},
\end{aligned} \tag{3}$$

where

$$\mathcal{H}(\xi,\xi_0) = \frac{\delta c G(\xi,\xi_0)}{c+\delta G(\xi,\xi_0)(K\delta c + b(\Lambda(\xi,\xi_0)+b\delta\theta))}. \tag{4}$$

Here h is the coefficient of the heat exchange with the environment which is prescribed via Newton's law of cooling, θ_e is the temperature of the environment which is assumed to be constant, c is the heat capacity coefficient of the SMA, and ξ_0 represents the value of ξ at the end of the previous phase transformation. It should be noted that the model [2] allows one to describe the temperature changes as the result of two competing processes, the heat generation resulting from the phase transformations represented by the first term, and the heat exchange with the environment (second term). The explicit expressions and explanations of the functions $\Lambda(\xi,\xi_0)$ and $G(\xi,\xi_0)$ are given in Appendix A.

In order to carry out effective numerical calculations, the system (3) was non-dimensionalized, using the non-dimensional variables and parameters as follows:

$$\tau = \alpha t, \quad \alpha = \sqrt{\frac{K}{m}}, \quad \omega = \frac{\Omega}{\alpha}, \quad \hat{x} = \frac{x}{x_{M_s}}, \quad \hat{g} = \frac{g}{x_{M_s}}, \quad \eta = \frac{\mu}{2\alpha m},$$

$$k_1 = \frac{K_1}{K}, \quad \rho = \frac{A}{x_{M_s}}, \quad \hat{\theta} = \frac{\theta}{\theta_e}, \quad \lambda = \frac{K\delta}{f_{M_s}},$$
$$J = \frac{b\theta_e}{f_{M_s}}, \quad L = \frac{b\delta}{c}, \quad \hat{h} = \frac{h}{c\alpha}.$$

Here f_{M_s} and x_{M_s} are the pseudoelastic force and the displacement at the onset of the upper pseudoelastic plateau in Fig. 1a. For the convenience, the hats will be omitted for the system non-dimensional variables and they will be referred to as x, θ and parameters h, g. Then the non-dimensional system of equations for the pseudoelastic oscillator can be written in the following form:

$$\begin{aligned}
&\dot{x} = v,\\
&\dot{v} = -k_1 x - 2\eta v - (x+g-\lambda\xi\,\mathrm{sign}(x+g))\mathrm{H}(-x-g) + \rho\omega^2\cos(\omega\tau),\\
&\dot{\xi} = \overline{\mathcal{H}}(\xi,\xi_0)(v\ \mathrm{sign}(x+g) - Jh(1-\theta))\mathrm{H}(-x-g),\\
&\dot{\theta} = L\frac{\overline{\Lambda}(\xi,\xi_0)+J\lambda\theta}{J\lambda}\overline{\mathcal{H}}(\xi,\xi_0)(v\ \ \mathrm{sign}(x+g) - Jh(1-\theta))\mathrm{H}(-x-g)) + h(1-\theta),
\end{aligned} \tag{5}$$

The functions $\overline{\mathcal{H}}(\xi,\xi_0)$, $\overline{\Lambda}(\xi,\xi_0)$ and $\overline{G}(\xi,\xi_0)$ are non-dimensional versions of functions $\mathcal{H}(\xi,\xi_0)$, $\Lambda(\xi,\xi_0)$ and $G(\xi,\xi_0)$, and they can be found in Appendix B.

The oscillating mass can impact the SMA constrain; depending on the impact strength and duration, five different modes of operation can be distinguished:

- *Mode I*. Light contact without phase transformations (austenite elastic behaviour).
- *Mode II*. Contact with forward phase transformation.
- *Mode III*. Contact when material is completely in martensite phase (martensite elastic behaviour).
- *Mode IV*. Contact with reverse transformation.
- *Mode V*. No contact.

An example of such sequence for one period of motion is presented in Fig. 3, where displacement, martensite volume fraction, temperature and force f_{pe} are monitored for all five different modes.

The detailed description of all modes, containing equations of motion for each of them can be found in [15]. Here we give just a brief summary of the processes taking place throughout the modes. From Mode I to Mode IV the motion occurs when the mass and the SMA restraint are in contact. At a certain strength of the impact, phase transformations take place. That leads to the changes of temperature and of internal variable ξ. The evolution

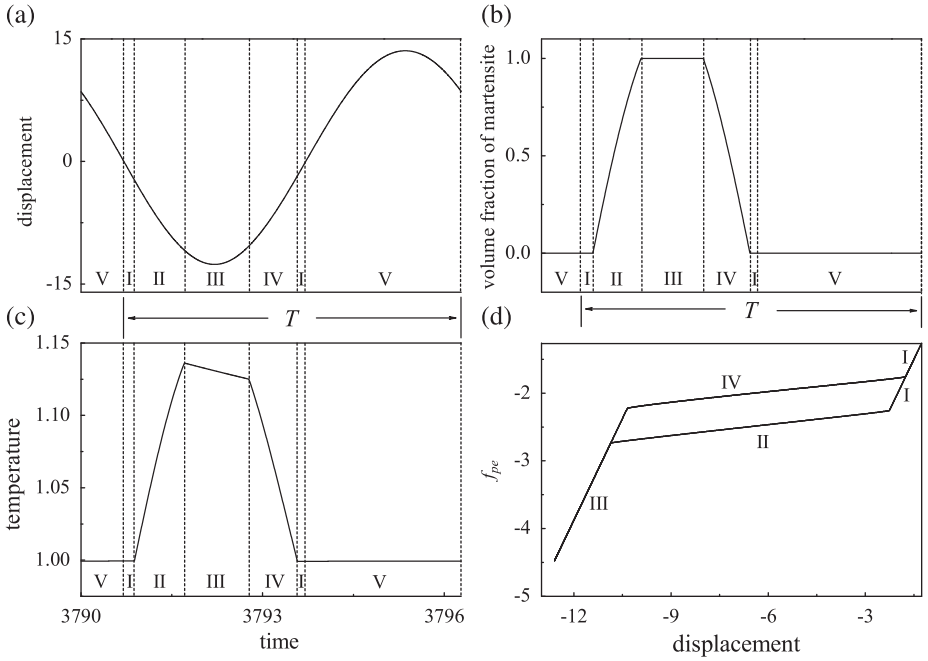

Fig. 3. Time histories and hysteresis loop of the oscillator impacting the SMA constraint. (a) and (c) show the mass displacement and the SMA temperature over one excitation period, T. (b) and (d) depict the corresponding changes of volume fraction of martensite, ξ, and dependence of the pseudoelastic force, f_{pe} on the displacement (hysteresis loop).

Table 1
Contact modes of motion.

Mode	f_{pe} boundaries	f_{pe} explicit expression	Internal variable ξ	Temperature variations
I	$\|f_{pe}\| < f_{M_s}$	$f_{pe} = x+g$	$\xi = 0, \dot{\xi} = 0$	$\dot{\theta} = h(1-\theta)$
II	$f_{M_s} \le \|f_{pe}\| \le f_{M_f}$	$f_{pe} = x+g+\lambda\xi$	$\dot{\xi} \ge 0$	$\dot{\theta} = \Phi(\xi, \xi_0, \vartheta)\dot{\xi} + h(1-\theta)$
III	$\|f_{pe}\| > f_{M_f}$ when $\dot{v} < 0$ $\|f_{pe}\| > f_{A_s}$ when $\dot{v} > 0$	$f_{pe} = x+g+\lambda$	$\xi = 1, \dot{\xi} = 0$	$\dot{\theta} = h(1-\theta)$
IV	$f_{A_f} \le \|f_{pe}\| \le f_{A_s}$	$f_{pe} = x+g+\lambda\xi$	$\dot{\xi} \le 0$	$\dot{\theta} = \Phi(\xi, \xi_0, \vartheta)\dot{\xi} + h(1-\theta)$

of these variables along with the explicit expression of the pseudoelastic element restoring force $f_{pe} = (x+g-\text{sign}(x+g)\lambda\xi)$ for each mode are given in Table 1. The function $\Phi(\xi, \xi_0, \vartheta)$ in the temperature equation represents the temperature variations associated with the phase transformations, that is

$$\Phi(\xi, \xi_0, \vartheta) = L\frac{\overline{A}(\xi, \xi_0) + J\lambda\theta}{J\lambda}. \tag{6}$$

No-contact Mode V is the simplest case for which the dynamic responses of the oscillator are governed by the linear primary spring and damper. As a result, $f_{pe} = 0$ and because of that there are no phase transformations and the condition $\xi = 0$ holds true for Mode V. The temperature change in the SMA is defined by the heat exchange with the environment.

The other modes (Modes I to IV) describe the SMA response for the two complete phase transformations, from austenite to martensite during loading and the reverse transformation for unloading. However, if the force acting on the discontinuous support is not high enough to induce the complete transformation, a partial phase transformation can occur. This behaviour is called an internal sublooping. In this case, the internal variable reaches an intermediate value of ξ_0, when loading of the SMA element. On a subsequent unloading, a reverse transformation is initiated when the pseudoelastic force reaches the limit, which is the function of $\Psi_F(1, \xi_0)$ and the current temperature of the SMA.

3. Numerical results

The interest in use of SMAs in vibrational systems is stimulated by their ability to dissipate energy and consequently their potential to control the dynamic behaviour of the system. The present study aims to assess the applicability of SMA for vibration reduction and this will be accomplished by comparing of the dynamic responses computed for the elastic and pseudoelastic impact oscillators.

The values of the material parameters used in the current numerical investigations were taken from [2] and they are as follows: $h = 0.08$, $L = 0.124$, $J = 3.1742$, $\lambda = 8.125$, $a = 0.03$. Such a choice corresponds to a pseudoelastic loop with a "medium" level of hysteresis and slope of the pseudoelastic plateaus. Along with the system parameters $k_1 = 0.03448$, $\eta = 0.01$ and $g = 1.26$ they are kept constant, which allows us concentrate on the effects caused by the variation of the external loading parameters (excitation frequency and amplitude).

3.1. Damping effect of the SMA impact constraint

It is widely accepted that the pseudoelastic SMAs possess significant damping properties due to the presence of hysteresis. Our numerical study of the impact oscillator shows that the

damping effect of the SMA can be very significant. Fig. 4 depicts bifurcation diagrams for the considered oscillators with elastic (in black) and pseudoelastic (in red) constraints under varying excitation frequency ω. As can be seen, a large variety of periodic and chaotic responses are observed in both cases, and there are several regions where the bifurcation diagrams coincide. This means that in these regions the intensity of the impact force acting on the SMA constraint is not high enough to initiate the phase transformations, and therefore the SMA element acts as a linear spring. The differences in the responses in the other ranges of frequencies are caused by phase transformations.

It can be seen from Fig. 4 that for both elastic and pseudoelastic oscillators as the frequency increases, a number of "resonance" peaks are observed. For the considered range, $\omega \in (0, 1.8)$, five clear regions with large amplitude of the vibration are obtained for the elastic oscillator. It should be noted that the system response is periodic in these frequency ranges and the periodicity of the response is increasing for each consecutive region varying from period-1 for $\omega \in (0.145, 0.394)$ to period-5 for $\omega \in (1.242, 1.551)$. However, for the pseudoelastic oscillator the amplitude of the response in these regions is significantly smaller than that for the elastic oscillator. It was found that in those regions, i.e. for $\omega \in (0.786, 0.932)$, $\omega \in (1.097, 1.121)$ and $\omega \in (1.198, 1.55)$, the co-existence of the periodic responses was observed for the pseudoelastic oscillator, whereas elastic oscillator exhibited single periodic response. The characteristic behaviour of the system is described below for the second and forth peak regions which were chosen as representative examples.

First we consider the frequency range, $\omega \in (0.511, 0.623)$, where the second "resonance" peak is observed. Here the period-2 response is seen which is very similar at $\omega \in (0.511, 0.533)$ for both system. However, at $\omega \in (0.533, 0.623)$ the behaviour of the elastic and pseudoelastic oscillators are different. Figs. 5a–e show an evolution of the period-2 attractors for both systems using Poincaré

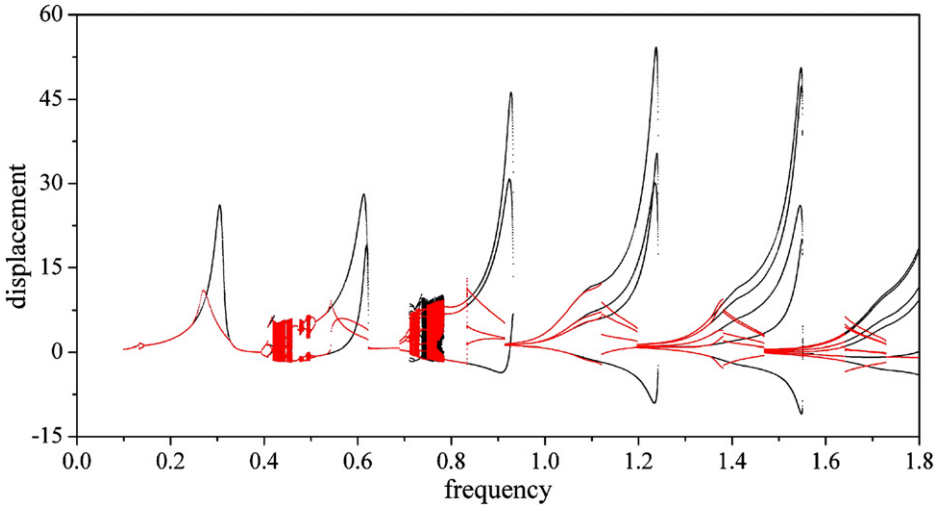

Fig. 4. Bifurcation diagrams for the increasing frequency ω computed for the elastic (black) and pseudoelastic (red) oscillators calculated at $\rho = 1.2$ (colour online).

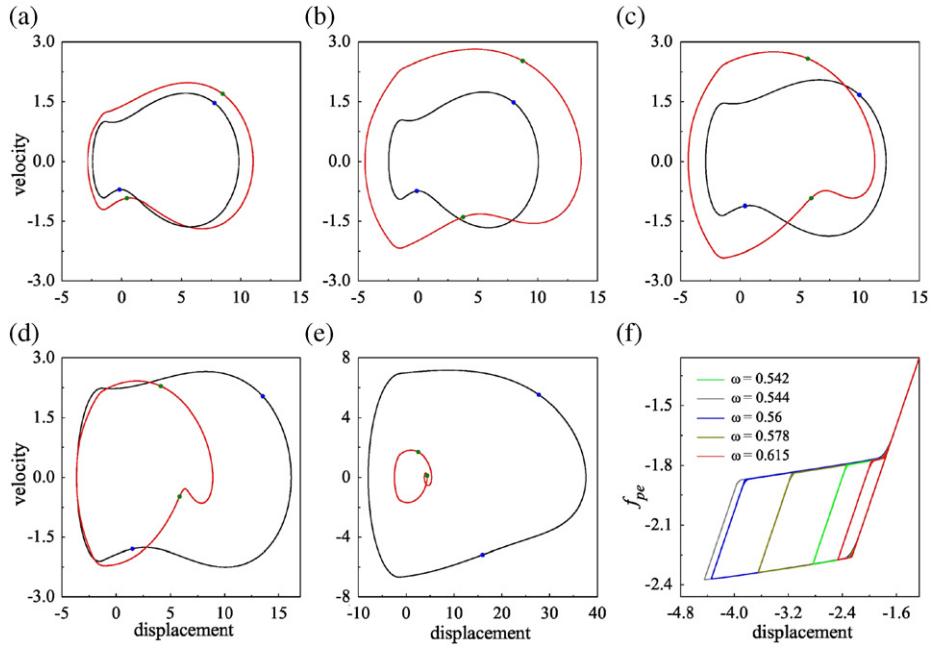

Fig. 5. Trajectories and Poincaré maps calculated for $\rho = 1.2$ and (a) $\omega = 0.542$; (b) $\omega = 0.544$; (c) $\omega = 0.56$; (d) $\omega = 0.578$; (e) $\omega = 0.615$ and (f) hysteresis loops for those frequency values. In (a)–(e) red and black curves show the responses of the pseudoelastic and elastic oscillator, respectively (colour online).

sections and trajectories plotted at the increasing frequency values in black for the elastic oscillator and in red for the pseudoelastic one. In this frequency range there are three types of typical behaviours. Initially, the occurrence of phase transformations in the SMA leads to the increase in the amplitude of the response for the pseudoelastic oscillator as compared to the elastic oscillator (see Figs. 5a and b calculated for $\omega = 0.542$ and 0.544, respectively). This can be explained by the initiation of phase transformations in the pseudoelastic constraint, which causes change in the stiffness of the SMA, making it "softer", and leads to the larger displacement of the secondary support and the mass accordingly. It consequently prolongs the time of the contact, causing "sticking" of the mass to the discontinuous constraint. For this range the area of the hysteresis loop also increases with the frequency, as can be seen in Fig. 5f. With further increase of frequency, the response amplitude for the elastic oscillator starts to grow rapidly, whereas the pseudoelastic oscillator response amplitude decreases. After $\omega = 0.557$ (see Fig. 5c for $\omega = 0.56$) the positive displacements for the elastic oscillator are larger than the ones of the pseudoelastic oscillator; however, the displacement in the impact area remains larger for the pseudoelastic oscillator up to $\omega = 0.578$ (see Fig. 5d) for which the two are similar. Finally, at even higher values of frequency the response amplitude for the elastic oscillator becomes larger than that of the pseudoelastic oscillator as it is demonstrated in Fig. 5e where phase space for the frequency value $\omega = 0.615$ is shown. At the same time the decrease in the size of hysteresis loop is observed as demonstrated in the Fig. 5f. Our analysis shows that for the pseudoelastic oscillator, the impact strength decreases as the frequency increases, and starting from $\omega = 0.578$, the deformation of the constraint becomes smaller than the one for the elastic oscillator. Thus, for the considered frequency range and other specified parameters, the vibration reduction can be achieved for $\omega \in (0.578, 0.623)$.

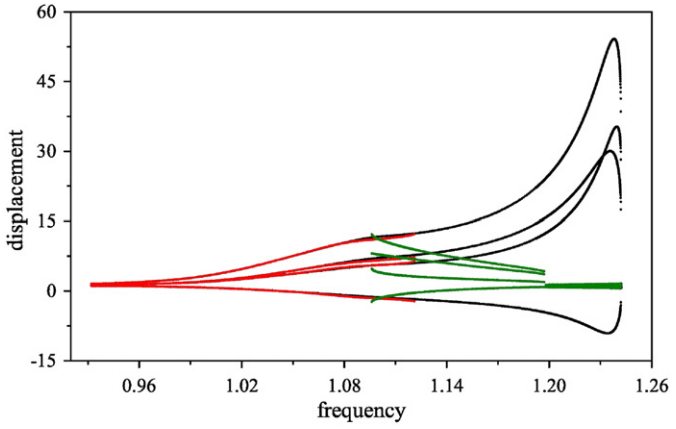

Fig. 6. Bifurcation diagrams showing displacement as function of the excitation frequency at $\omega \in (0.932, 1.242)$ and $\rho = 1.2$ (colour online).

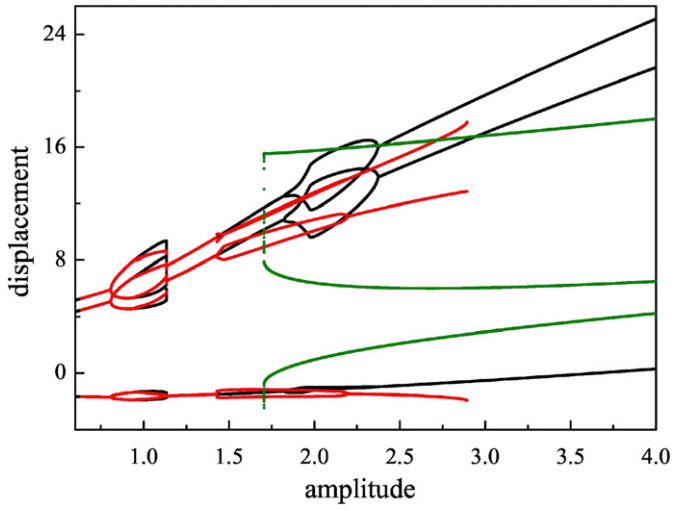

Fig. 8. Bifurcation diagrams showing displacement as function of the excitation amplitude for $\rho \in (0.6, 4.0)$ and $\omega = 0.805$ (colour online).

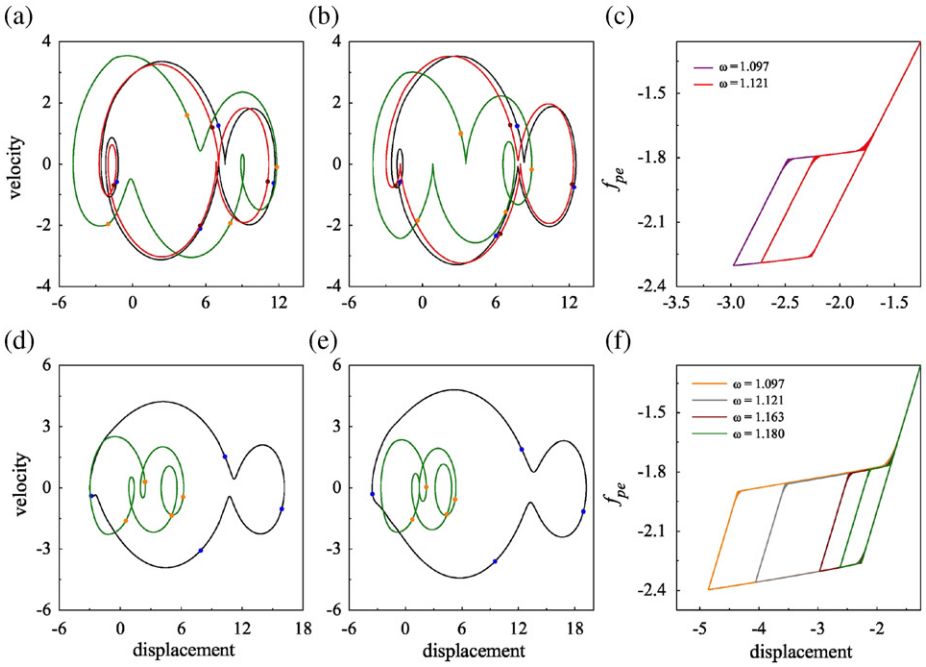

Fig. 7. Trajectories and Poincaré maps computed for $\rho = 1.2$ and (a) $\omega = 1.097$; (b) $\omega = 1.121$; (d) $\omega = 1.163$; (e) $\omega = 1.18$; and hysteresis loops for (c) the red attractor and (f) the green attractor for different frequency values. In (a), (b), (d), (e) red and green curves show the responses of the pseudoelastic oscillator and the black curve shows the response of the elastic oscillator (colour online).

As can be seen from Fig. 4, for the higher frequency values at the "resonance" peaks there is a number of characteristic jumps in the bifurcation diagram for the pseudoelastic oscillator, which indicates presence of the co-existing attractors in the system. This typical behaviour is presented in Fig. 6, where the bifurcation diagrams of two co-existing regimes for the pseudoelastic oscillator (in red and green) and the response of the elastic oscillator (in black) are shown. It can be seen that two different period-4 responses coexist in the narrow range of frequency $\omega \in (1.097, 1.121)$. Poincaré sections and trajectories of these coexisting responses are shown in Figs. 7a and b for the frequency values $\omega = 1.097$ and 1.121, respectively, along with the elastic oscillator response shown in black. It should be noted here that the red attractor of the pseudoelastic oscillator is very similar to the attractor of the elastic oscillator, and its hysteresis loop grows in size with the increase of frequency as shown in Fig. 7c. In general, the strength of impacts for this attractor is just slightly larger than for purely elastic impacts. The second (green) attractor, however, differs significantly from the one corresponding to the elastic oscillator, and the strength of the impact is significantly larger at $\omega \in (1.097, 1.163)$. At $\omega = 1.097$ (see Fig. 7a), for which this regime comes into existence, the span of the oscillations is larger in comparison with the elastic one, but soon after that the amplitude of oscillations in positive direction for the elastic oscillator prevails. At $\omega = 1.163$ (see Fig. 7d) the impacts strength for both cases is the same and with further increase of frequency, the response amplitude for the elastic oscillator becomes clearly larger than that of the pseudoelastic oscillator, as it is shown in Fig. 7e. The hysteresis loop corresponding to this response shrinks for the increasing frequency; its evolution is shown in Fig. 7f. Therefore, in the frequency range considered, the vibration reduction cannot be achieved everywhere but only for $\omega \in (1.163, 1.241)$.

In both frequency ranges described above, it was observed that the vibration reduction is possible above a certain critical frequency value. Our numerical analysis confirmed that this is a common scenario, and the influence of the excitation amplitude ρ on the system responses was studied next. In general, the value of this critical frequency will vary as the amplitude increases. It is interesting to understand how the responses below and above this value will be modified under changing amplitude and this question is addressed below. Here the third "resonance" region $\omega \in (0.786, 0.932)$ is considered as an example. In this range, the vibration reduction is possible at frequencies higher than $\omega = 0.871$. To demonstrate the system behaviour a frequency below the critical value, i.e. $\omega = 0.805$, was selected, and the bifurcation diagram was constructed under varying amplitude as shown in Fig. 8. As before, the responses of the pseudoelastic oscillator are shown in green and red; the elastic oscillator response is shown in black. It can be seen that pseudoelastic responses co-exist in only limited range of amplitudes, namely for $\rho \in (1.705, 2.895)$. For higher amplitudes just one pseudoelastic response remains and its impact displacement is larger than that for the elastic oscillator. The evolution of these attractors is shown in Fig. 9, where the phase portraits for the elastic (black) and pseudoelastic (red) responses are similar, however, the SMA deformation is slightly larger. The amplitude of the green pseudoelastic attractor is larger than the elastic one for smaller amplitude values as shown in Fig. 9b, but as the forcing amplitude increases, the span of the oscillations is reduced and becomes smaller than its elastic counterpart. However, even in this case, the displacement of the constraint remains larger than that for the elastic oscillator due to the softening of the pseudoelastic element resulting from phase transformations. Consequently, for the frequency ranges where the pseudoelastic oscillator does not show the vibration reduction, this behaviour was retained for higher amplitudes of the external excitation.

For the frequencies above the critical value $\omega = 0.871$, it was obtained that a single period-3 response persists as the amplitude increases, and the response amplitude for the elastic oscillator remained larger than that for the pseudoelastic oscillator. Therefore, we conclude that vibration reduction behaviour observed in

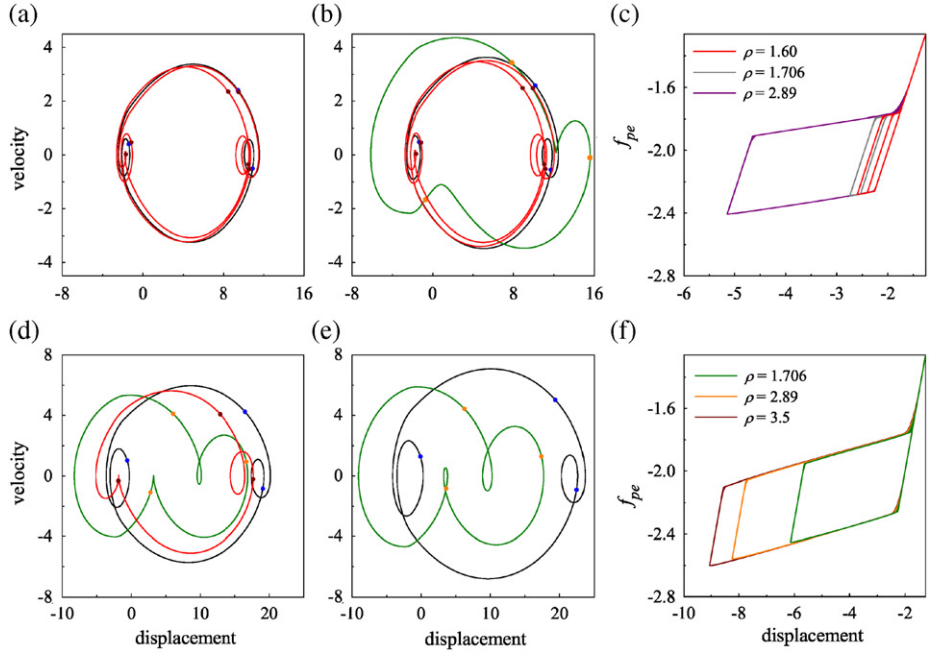

Fig. 9. Trajectories and Poincaré maps for $\omega = 0.805$ and (a) $\rho = 1.6$; (b) $\rho = 1.706$; (d) $\rho = 2.89$; (e) $\rho = 3.5$; and hysteresis loops for (c) the red attractor and (f) the green attractor for different amplitude values. In a,b,d,e red and green curves show the responses of the pseudoelastic oscillator and the black curve shows the response of the elastic oscillator (colour online).

the "resonance" regions is not affected by the variations in the excitation amplitude.

3.2. Influence of the phase transformations on the co-existing responses

Though a significant decrease in the span of periodic attractor makes pseudoelastic SMAs very promising for passive vibration control applications, it appears that such behaviour is not persistent and is observed in certain frequency ranges corresponding to "resonance" peaks. It is important to know that the presence of SMA in the impact systems can also modify existing regimes and can even cause new responses to be initiated as was demonstrated in the previous subsection. Careful monitoring of these new and modified regimes is especially important in those frequency regions where chaotic behaviour is observed. In order to emphasize the complexity of the dynamic regimes caused by the presence of the pseudoelastic non-linearity, and to point out the advantageous and potentially dangerous responses, the second chaotic region in Fig. 4 was examined.

Given the significant number of co-existing attractors for both systems, Fig. 10a presents bifurcation diagrams for the co-existing regimes of the elastic oscillator (in black, magenta and blue); Fig. 10b shows the co-existing regimes for the pseudoelastic oscillators (in red, purple and green). As it is seen for the pseudoelastic oscillator, the chaotic behaviour appears in the frequency range $\omega \in (0.7114, 0.7847)$, whereas for the elastic oscillator the chaotic response occurs in a narrower frequency range $\omega \in (0.7377, 0.785)$. Also, in the case of pseudoelastic oscillator, the chaotic region has several periodic windows in contrast to a single narrow periodic window for the elastic system. For $\omega \in (0.67, 0.7113)$ the blue attractor for the elastic oscillator coincides with the red attractor for pseudoelastic oscillator, which means that there no phase transformations occur at least for some sets of the initial conditions. However in the overlapping frequency range, $\omega \in (0.6671, 0.6985)$, another large amplitude attractor (shown in green) exists having significant phase transformations. This attractor can be periodic or chaotic depending on the frequency value. In addition, there is a different period-5 attractor with phase transformation at $\omega \in (0.6974, 0.7074)$. Thus the study of the co-existing regimes

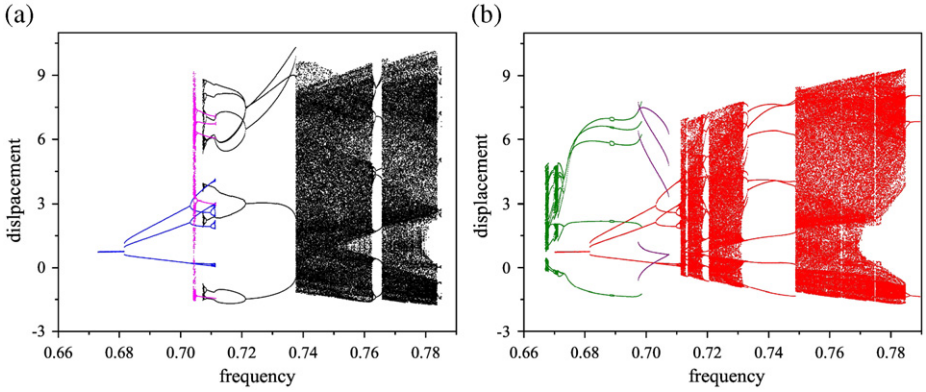

Fig. 10. Co-existence of the dynamic responses at $\omega \in (0.667, 0.7894)$ in form of bifurcation diagrams for (a) elastic oscillator and (b) pseudoelastic oscillators (colour online).

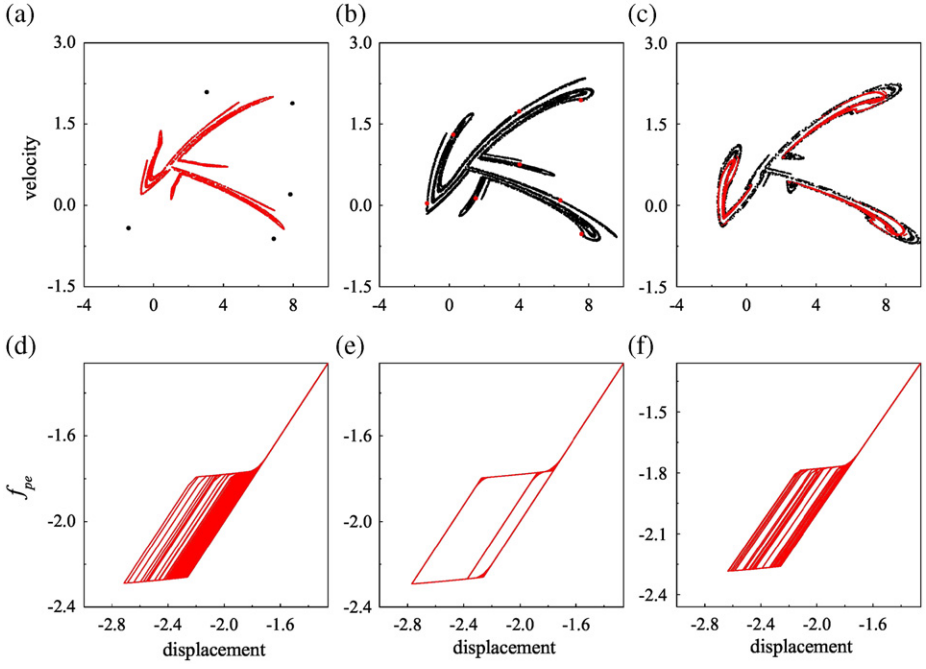

Fig. 11. Poincaré maps and hysteresis loops for $\omega = 0.725$ (plots (a),(d)); $\omega = 0.744$ (plots (b),(e)), $\omega = 0.777$ (plots (c),(f)) (colour online).

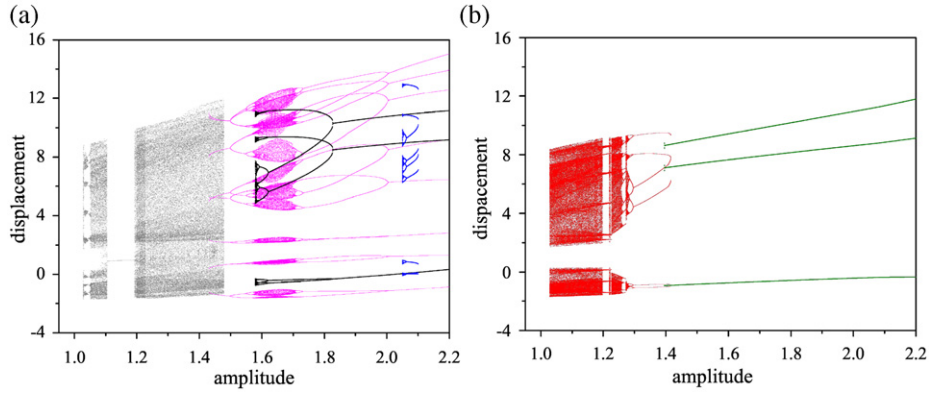

Fig. 12. Co-existence of the dynamic responses for $\omega = 0.775$ and $\rho \in (1.028, 2.2)$ in form of bifurcation diagrams for (a) elastic oscillator and (b) pseudoelastic oscillator (colour online).

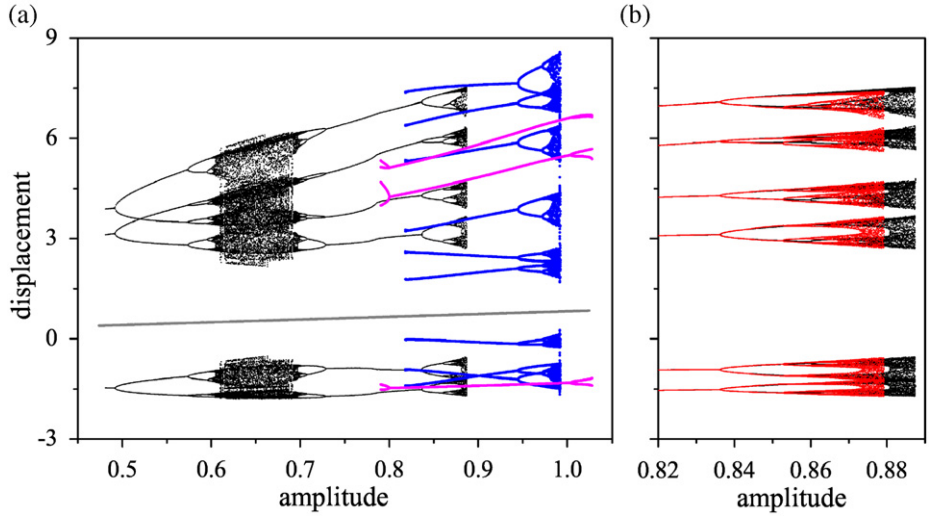

Fig. 13. Co-existence of the dynamic responses for $\omega = 0.775$ and $\rho \in (0.482, 1.028)$ (colour online).

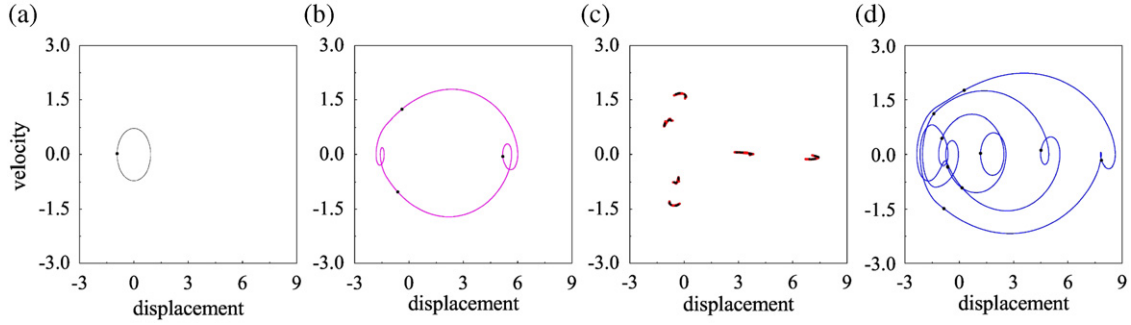

Fig. 14. Poincaré maps and trajectories calculated for $\rho = 0.775$, $\omega = 0.875$ (colour online).

for the pseudoelastic oscillator reveals that new attractors with stronger impacts are present in this frequency range, and it is not feasible to use SMA support for vibration reduction if the system is to operate in this range. Fig. 11 presents three different types of the response modification scenario, which were observed in this frequency range, where Poincaré sections are depicted in Figs. 11a–c and the corresponding pseudoelastic hysteresis loops are shown in Figs. 11d–f. In the first case calculated at $\omega = 0.725$ (Figs. 11a and d), the elastic oscillator has period-5 response, whereas pseudoelastic oscillator attractor is chaotic. At $\omega = 0.744$ the situation is opposite: the chaotic regime for the elastic oscillator is replaced by the period-8 response in the case of pseudoelastic oscillator (Figs. 11b,e). Finally, at $\omega = 0.777$ both systems have chaotic attractors (Figs. 11c, f), however the attractor shrinks for the pseudoelastic oscillator.

The evolution of the chaotic responses under varying excitation amplitude ρ was also considered. The bifurcation diagrams shown in Figs. 12a,b were calculated at the value of frequency $\omega = 0.775$ for the amplitude range $\rho \in (1.028, 2.2)$. As it can be seen, initially chaotic behaviour is observed for both elastic and pseudoelastic oscillators, though the span of the chaotic attractor for the pseudoelastic oscillator is smaller than that of the elastic

counterpart. However, with further increase of the excitation amplitude, the pseudoelastic oscillator shows a stable period-3 response, whereas for the elastic oscillator a variety of the complex co-existing responses, both periodic and chaotic, is observed. For low values of the excitation amplitude, $\rho \in (0.482, 1.027)$, the picture is more complex as it is evident from Figs. 13a and b. Initially the impact strength is insufficient to initiate phase transformations and both the elastic and pseudoelastic oscillators demonstrate the same response (shown in black). At $\rho = 0.852$ phase transformations are initiated in the pseudoelastic element and this leads to the difference in the responses for two oscillators (see Fig. 13b). The chaotic attractors for $\rho = 0.875$ are shown in Fig. 14c in red and black for the pseudoelastic and elastic oscillator, respectively. The period-3 response marked in magenta colour, as shown in Fig. 13a, is the same for both oscillators and its trajectory and attractor for $\rho = 0.875$ are shown in Fig. 14b. The response shown in blue for $\rho \in (0.819, 0.991)$ was observed only for the elastic oscillator, and the trajectory and attractor for this response for $\rho = 0.875$ are shown in Fig. 14d. Also, in the low amplitude range the no-contact period-1 response exists for both oscillators. It is shown in Fig. 13a in grey, and its trajectory and Poincaré map for $\rho = 0.875$ are presented in Fig. 14a.

The basins of attractions plotted for $\rho = 0.875$ and $\omega = 0.775$ are presented in Fig. 15 for the elastic (Fig. 15a) and the pseudoelastic (Fig. 15b) oscillators. The basins for the period-1, period-3 and chaotic attractors are shown in brown, orange and black, respectively. The basin for the period-9 response corresponding to the elastic oscillator is shown in light yellow. As it can be seen, the presence of the SMA decreases the fractality of the basin and eliminates one elastic response without replacing it by a new pseudoelastic regimes. An expansion of the chaotic region for the pseudoelastic oscillator is also noticeable.

It should be noted that the basins of attractions presented in Fig. 15 and other figures were calculated using Dynamics software [16] which allows to calculate a projection of the full basins on the two dimensional plane (in this case displacement/velocity plane). Due to software limitations variation of initial conditions for other system variables was not possible when calculating basins of attractions, hence we kept initial values $\xi = 0$, $\xi_0 = 0$ and $\theta = 1$ constant (θ was non-dimensionalized with respect to the ambient

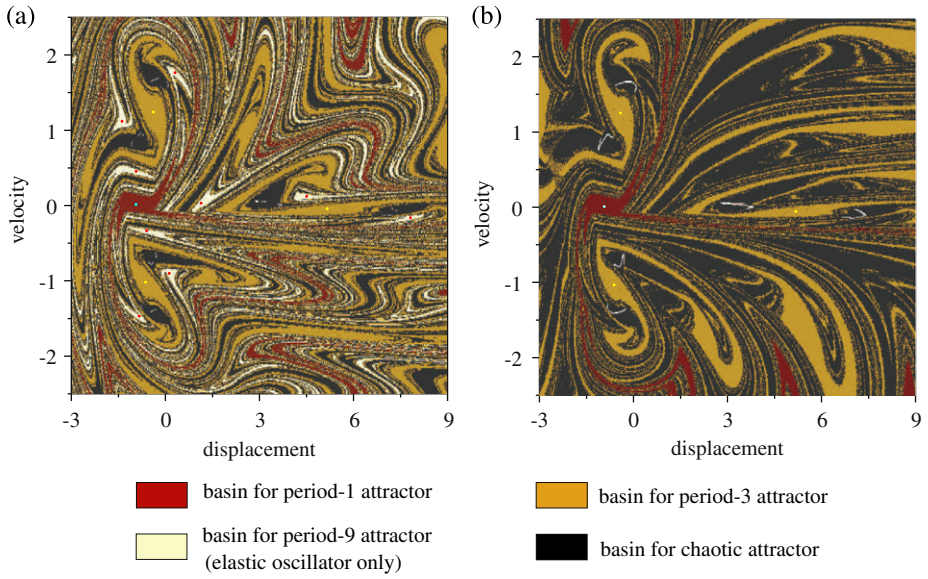

Fig. 15. Basins of attraction computed for $\rho = 0.875$ and $\omega = 0.775$: (a) elastic oscillator; (b) pseudoelastic oscillator (colour online).

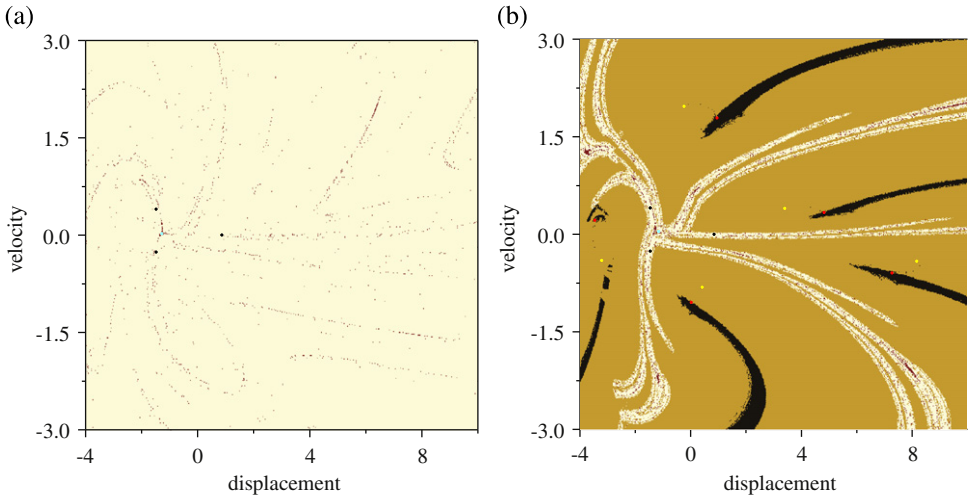

Fig. 16. Basins of attraction computed for $\rho = 1.2$ and $\omega = 0.698$: (a) elastic oscillator; (b) pseudoelastic oscillator (colour online).

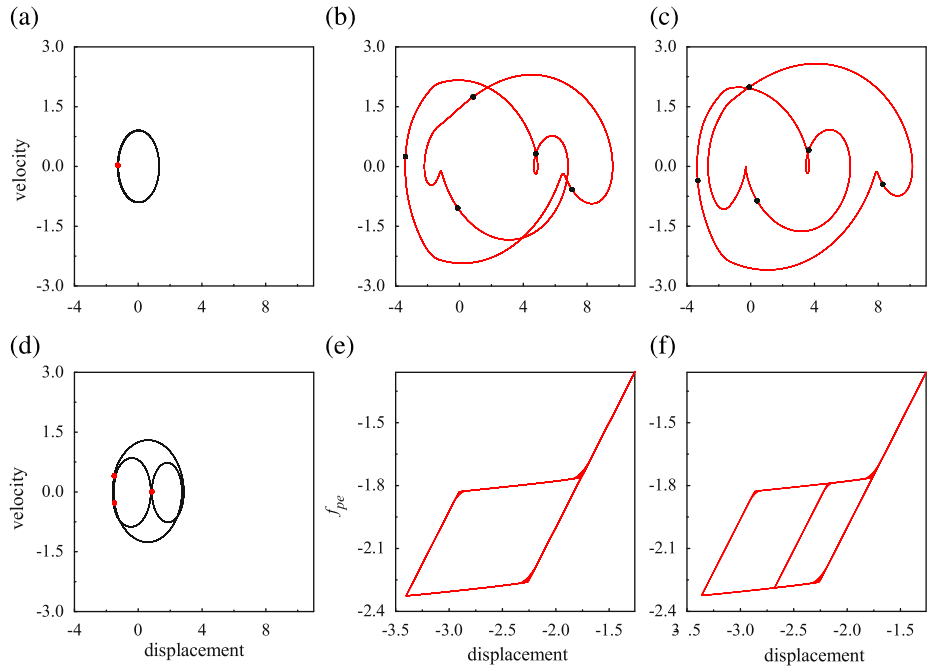

Fig. 17. Co-existing attractors shown as Poincaré maps and trajectories on the phase plane for $\rho = 1.2$ and $\omega = 0.698$: regimes which coincide for the oscillators with SMA and elastic constraints—plots (a), (d); regimes which exist only for pseudoelastic oscillator: period-5 orbit and hysteresis loop—plots (b), (e), period-5 orbit of larger amplitude and hysteresis loop—plots (c), (f) (colour online).

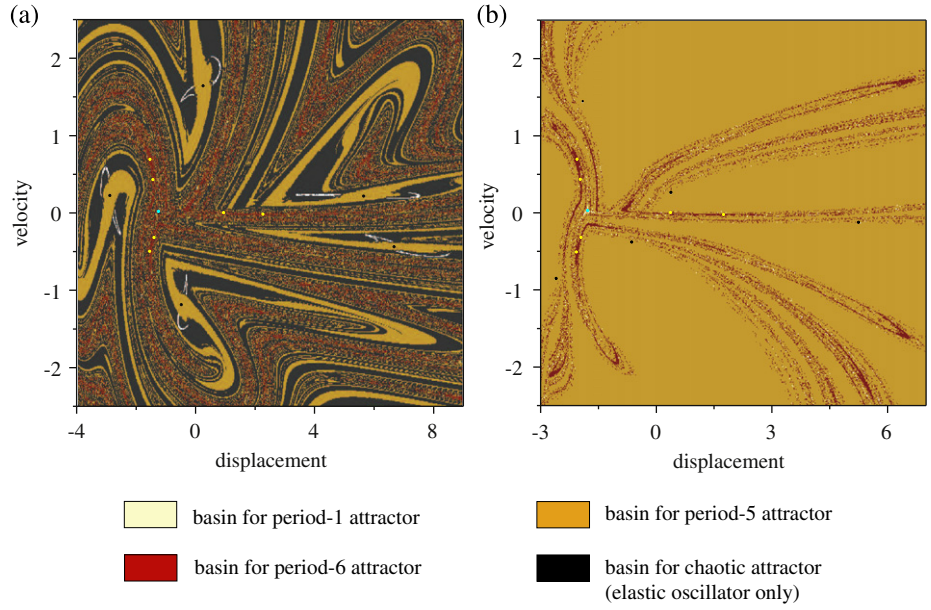

Fig. 18. Basins of attraction computed for $\rho = 1.2$ and $\omega = 0.7074$: (a) elastic oscillator; (b) pseudoelastic oscillator (colour online).

temperature). However, this approximation of the initial conditions for temperature and volume fraction of martensite does not influence the final results of the calculation, because during the iterations the system settles down quickly on the correct attractor, and its projection is then presented on the given basins plot.

Our numerical study shows that the presence of the SMA can introduce co-existing high amplitude responses, which do not exist for the equivalent elastic oscillator. To illustrate this effect and to demonstrate the overall complexity of the system behaviour, the basins of attractions are presented in Fig. 16 for the elastic (Fig. 16a) and the pseudoelastic (Fig. 16b) oscillators. Their trajectories are shown in Fig. 17. The low amplitude period-1 and period-3 responses shown in Figs. 17a and d in black, are the same for both oscillators; their basins of attraction are shown in brown and yellow in Fig. 16, respectively. Two period-5 orbits shown in Figs. 17b and c appear only for pseudoelastic oscillator as a result of phase transformations. The basin of attraction corresponding to the attractor depicted in Fig. 17c is marked in dark yellow. It is clearly dominant over the basin of other period-5 attractor, which trajectory and Poincaré map are shown in Fig. 17b. It should be noted that the transient motion for these responses is relatively short and the system settles on the relevant attractor after 50–100 cycles depending on the initial conditions. The presence of high amplitude responses can be dangerous and

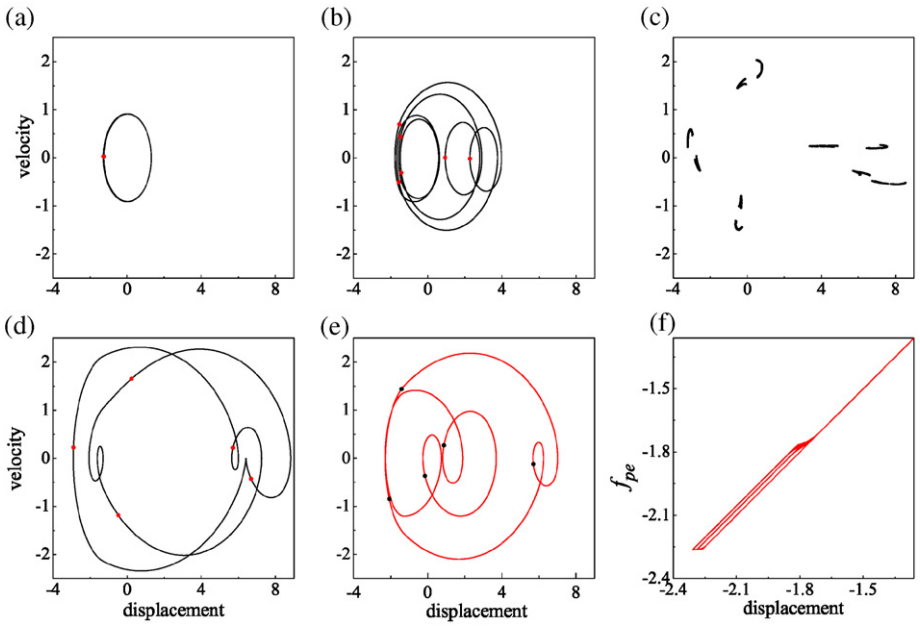

Fig. 19. Coexisting attractors shown as Poincaré maps and trajectories on the phase plane for $\rho = 1.2$ and $\omega = 0.7074$: (a,b) regimes which coincide for the oscillators with SMA and elastic constraints; (c) chaotic attractor for the elastic oscillator; (d) period-5 orbit for the elastic oscillator; (e,f) period-5 regime and the corresponding hysteresis loop for pseudoelastic oscillator (colour online).

therefore the existence of such regimes due to the phase transformation in the SMA must be taken into account.

Different scenario is shown in Fig. 18 where basins of attraction are presented for the elastic (Fig. 18a) and the pseudoelastic (Fig. 18b) oscillators for $\rho = 1.2$ and $\omega = 0.7074$. Their trajectories are shown in Fig. 19. As it can be seen, for these values of the parameters, four different regimes exist for the elastic oscillator, whereas pseudoelastic oscillator has only three different responses. Two low amplitude periodic responses shown in Figs. 19a and b are the same for pseudoelastic and elastic oscillators. However, high amplitude chaotic and period-5 responses for the elastic oscillator (Figs. 19c and d) are replaced and by a single period-5 lower amplitude response for the pseudoelastic oscilator (Fig. 19e).

4. Conclusions

The influence of the external excitation parameters on the dynamic behaviour of an impact oscillator with SMA motion constraint was studied. The thermo-mechanical model proposed in [1,2] was adopted to account the phase transformations in the SMA element including the thermo-mechanical coupling terms in the energy equation. The oscillator can operate in five different modes of motion, and the most essential details of the processes taking place throughout each mode were discussed. In order to assess potentials of the system to be used for vibration reduction, a comparison with the equivalent elastic impact oscillator was carried out.

The evolution of the dynamic responses under varying frequency was investigated first. The analysis has shown that a significant vibration reduction can be achieved for the frequency ranges corresponding to the "resonance" peaks which are inherent to the considered elastic impact oscillator. For each peak a certain critical frequency was identified, where the impact displacements of the elastic and pseudoelastic oscillators coincide, and the vibration reduction was obtained for the frequencies above this value. At the frequencies below this value, the response amplitudes for the pseudoelastic oscillator were larger than that for the elastic counterpart. This can be explained by softening of the SMA constraint during the phase transformation, which causes larger impact displacements. Also, for the third, forth and fifths peaks a single periodic response for the elastic oscillator was replaced by two co-existing responses for the pseudoelastic oscillator. The study of the excitation amplitude influence on the system responses revealed that vibration reduction behaviour observed in the "resonance" regions is not affected by the variations in the excitation amplitude. This means that for the frequencies below critical value the vibration reduction cannot be achieved by increasing the excitation amplitude.

At ranges of frequencies in between of those corresponding to the "resonance" peak regions an unexpected dynamic behaviour was observed. The presence of the SMA constraint alters the dynamics responses when compared to the ones from the elastic oscillator. Some of them are beneficial, such as the transformation of chaotic responses to periodic ones and the shrinkage of chaotic attractors. Also, some of the dangerous responses observed for the elastic oscillator were eliminated in case of the pseudoelastic oscillator. On the other hand, the existence of additional modes in the pseudoelastic oscillator can cause new large amplitude responses (both periodic and chaotic) to be generated. The effects of the external amplitude variations were also studied for the chaotic regions. In appeared that at high amplitude values the chaotic response transforms to the periodic one, and its periodicity is the same as of the following resonance peak response. Therefore, the increase of the amplitude at the considered frequency ranges leads to the elimination of the chaotic responses thus expanding "resonance" peak regions. Overall, the complexity and the unpredictability of the dynamic responses in the considered "chaotic" regions make the use of the SMA in the restraint generally disadvantageous for the vibration reduction purposes in these regions.

Appendix A

The function $\Lambda(\xi, \xi_0)$ is a piecewise smooth function which defines the shape and the size of the hysteresis loop, and according to the common assumption, the rate of energy

dissipation Γ during the transformation is proportional to this function, i.e. the size of the hysteresis loop, as defined in [1]

$$\Gamma = \Lambda(\xi, \xi_0)\dot{\xi}, \tag{7}$$

where

$$\Lambda(\xi, \xi_0) = \begin{cases} \Lambda_F = b\delta[(A_s - M_s)/2 - (M_s - M_f)\Psi_F(\xi, \xi_0)/\ln(a/(2-a))] & \text{if } \dot{\xi} > 0, \\ \Lambda_R = b\delta[-(A_s - M_s)/2 - (A_f - A_s)\Psi_R(\xi, \xi_0)/\ln(a/(2-a))] & \text{if } \dot{\xi} < 0, \end{cases} \tag{8}$$

and

$$\Psi_F(\xi, \xi_0) = \frac{1}{2}\ln\left[\frac{(2-a)(\xi - \xi_0) + a(1-\xi)}{a(\xi - \xi_0) + (2-a)(1-\xi)}\frac{(2-a)}{a}\right],$$
$$\Psi_R(\xi, \xi_0) = \frac{1}{2}\ln\left[\frac{a(\xi - \xi_0) - (2-a)\xi}{(2-a)(\xi - \xi_0) - a\xi}\frac{a}{(2-a)}\right]. \tag{9}$$

The functions Ψ_F and Ψ_R define the shape of the upper and lower plateaus of the hysteresis loop. The smoothness of the transition between elastic and pseudoelastic part of the hysteresis loop is governed by the coefficient a.

The function $G(\xi, \xi_0)$ in Eq. (4) is an auxiliary function which is defined as follows:

$$G(\xi, \xi_0) = \begin{cases} G_F = (d\Lambda_F/d\xi)^{-1} & \text{if } \dot{\xi} > 0. \\ G_R = (d\Lambda_R/d\xi)^{-1} & \text{if } \dot{\xi} < 0. \\ 0 & \text{if } \dot{\xi} = 0. \end{cases} \tag{10}$$

Appendix B

The auxiliary functions $\Lambda(\xi, \xi_0)$, $G_F(\xi, \xi_0)$ in Eqs. (3) have dimensions of energy, and they were normalized with respect to product $f_{M_s}x_{M_s}$. This leads to the explicit expressions of their non-dimensional counterparts as follows:

$$\overline{\Lambda}_F(\xi, \xi_0) = (J-1)\lambda\left[\frac{q_2 - 1}{2} - \frac{(1-q_1)\Psi_F(\xi, \xi_0)}{\ln\frac{a}{2-a}}\right],$$
$$\overline{\Lambda}_R(\xi, \xi_0) = (1-J)\lambda\left[\frac{q_2 - 1}{2} - \frac{q_2(1-q_3)\Psi_R(\xi, \xi_0)}{\ln\frac{a}{2-a}}\right], \tag{11}$$

$$\overline{G}_F(\xi, \xi_0) = \frac{\ln\frac{a}{2-a}}{\lambda(J-1)(1-q_1)\Psi'_F(\xi, \xi_0)},$$
$$\overline{G}_R(\xi, \xi_0) = \frac{\ln\frac{a}{2-a}}{\lambda(J-1)q_2(q_3-1)\Psi'_R(\xi, \xi_0)}, \tag{12}$$

where

$$q_1 = \frac{M_f}{M_s}, \quad q_2 = \frac{A_s}{M_s}, \quad q_3 = \frac{A_f}{A_s}. \tag{13}$$

The function $\mathcal{H}(\xi, \xi_0)$ was non-dimensionalized with respect to force f_{M_s} and its non-dimensional expression is as follows:

$$\overline{\mathcal{H}}(\xi, \xi_0) = \frac{\lambda\overline{G}(\xi, \xi_0)}{1 + \lambda^2 + L(\overline{\Lambda}(\xi, \xi_0) + J\lambda\vartheta)\overline{G}(\xi, \xi_0)}. \tag{14}$$

References

[1] D. Bernardini, T. Pence, Models for one-variant shape memory materials based on dissipation functions, International Journal of Non-Linear Mechanics 37 (2002) 1299–1317.
[2] D. Bernardini, G. Rega, Thermomechanical modelling, nonlinear dynamics and chaos in shape memory oscillators, Mathematical and Computer Modelling of Dynamical Systems 11 (3) (2005) 291–314.
[3] R.A. Ibrahim, Recent advances in nonlinear passive vibration isolators, Journal of Sound and Vibration 314 (3–5) (2008) 371–452.
[4] K. Williams, G. Chiu, R. Bernhard, Adaptive-passive absorvers using shape-memory alloys, Journal of Sound and Vibration 249 (5) (2002) 835–848.
[5] S. Saadat, J. Salichs, M. Noori, Z. Hou, H. Davoodi, I. Bar-On, Y. Suzuki, A. Masuda, An overview of vibration and seismic applications of NiTi shape memory alloy, Smart Materials and Structures 11 (2) (2002) 218–229.
[6] M.A. Savi, P.M.L.C. Pacheco, Chaos and hyperchaos in shape memory systems, International Journal of Bifurcation and Chaos 12 (3) (2002) 645–657.
[7] W. Lacarbonara, D. Bernardini, F. Vestroni, Nonlinear thermomechanical oscillations of shape-memory devices, International Journal of Solids and Structures 41 (5-6) (2004) 1209–1234.
[8] W. Lacarbonara, F. Vestroni, Nonclassical responses of oscillators with hysteresis, Nonlinear Dynamics 32 (2003) 235–258.
[9] M.A. Iadicola, J.A. Shaw, An experimental method to measure initiation events during unstable stress-induced martensitic transformation in a shape memory alloy wire, Smart Materials and Structures 16 (2007) 155–169.
[10] F. Auricchio, A. Reali, U. Stefanelli, A three-dimensional model describing stress-induced solid phase transformation with permanent inelasticity, International Journal of Plasticity 23 (2007) 207–226.
[11] J.A. Shaw, S. Kyriakides, Thermomechanical aspects of Ni–Ti, Journal of the Mechanics and Physics of Solids 42 (8) (1995) 1243–1281.
[12] D.C. Lagoudas, L.G. Machado, M. Lagoudas, Nonlinear vibration of a one-degree of freedom shape memory alloy oscillator: a numerical–experimental investigation, Proceedings of the AIAA Conference, 2005.
[13] S. Seelecke, Modeling the dynamic behavior of shape memory alloys, International Journal of Non-linear Mechanics 37 (8) (2002) 1363–1374.
[14] B.C. dos Santos, M.A. Savi, Nonlinear dynamics of nonsmooth shape memory alloy oscillator, Chaos, Solitons and Fractals, 40 (1) (2009) 197–209.
[15] E. Sitnikova, E. Pavlovskaia, M. Wiercigroch, Dynamics of an impact oscillator with SMA constraint, European Physical Journal—Special Topics 165 (2008) 229–238.
[16] H.E. Nusse, J.A. Yorke, Dynamics: Numerical Explorations, Springer, New York, 1998.